Ionics (2020) 26:6255–6264
https://doi.org/10.1007/s11581-020-03744-w

ORIGINAL PAPER

Tailored synthesis of hybrid iron-nitrogen-graphene with reduced carbon xerogel as an efficient electrocatalyst towards oxygen reduction

S. Seetharaman[1] · S. Vinod Selvaganesh[1] · Raghuram Chetty[1]

Received: 20 May 2020 / Revised: 17 July 2020 / Accepted: 14 August 2020 / Published online: 21 August 2020

Abstract

In this study, a non-precious metal-based electrocatalyst consisting of nitrogen-doped iron-coated reduced graphene oxide (FeNG) on carbon xerogel towards oxygen reduction reaction (ORR) in alkaline media is reported. Herein, we describe a facile three-step synthesis route towards enhanced ORR activity. The effect of pyrolysis temperature and the resulting structural variations of the designated catalyst towards ORR were investigated. The as-synthesized carbon xerogel samples were reduced (rC_X) and then pyrolyzed at different temperatures, viz., 700, 900, and 1100 °C, followed by the incorporation of FeNG, and their performance towards ORR was studied. The resultant rC_XFeNG (reduced carbon xerogel-iron-nitrogen-doped graphene) catalyst pyrolyzed at an optimum temperature of 1100 °C (rC_XFeNG-1100) showed enhanced electrocatalytic performance towards ORR and exhibited an onset potential of 0.84 V vs. RHE (reversible hydrogen electrode). Besides, it is remarkable that rC_XFeNG-1100 delivers a limiting current density of 5.55 mA cm^{-2}, which is fairly equivalent to that of the commercial Pt/C electrocatalyst. It is noteworthy that the rC_XFeNG-1100 electrocatalyst showed a four-electron transfer pathway for ORR and showed better stability and improved durability outperforming the commercial Pt/C electrocatalyst. The present study opens up a promising approach for the design and fabrication of cost-effective non-precious ORR electrocatalysts for alkaline polymer electrolyte fuel cells.

Keywords Carbon xerogel · Nitrogen doping · Reduced graphene oxide · Non-precious electrocatalyst · Oxygen reduction reaction · Alkaline fuel cells

Introduction

The judicious development of cost-effective and efficient electrocatalysts for oxygen reduction reaction (ORR) can substantially bring down the cost of fuel cells, and non-precious metal-based electrocatalysts (NPMCs) are being considered an alternative in this regard. In fact, the high cost, less availability of Pt, and relatively sluggish ORR kinetics in the acidic medium have turned the researchers' attention towards the alkaline medium and subsequently led to the development of alkaline polymer electrolyte fuel cells (APEFCs).

APEFCs are reported to exhibit superior characteristics over proton exchange membrane fuel cells (PEMFCs) especially in regard to kinetics at the cathode as well as ohmic polarization. Even when standard Pt catalysts [1, 2] are employed, ORR kinetics are inherently more facile in an alkaline medium as opposed to acidic conditions. This permits the use of non-noble and low-cost metals such as iron and nickel as electrocatalysts in APEFCs instead of necessarily using Pt as is the case in PEMFCs [3, 4]. Hence, APEFCs are regarded as a suitable low-cost technology to address the energy demands of various applications.

Recently, carbon-based catalysts are reported to show promising ORR activity in alkaline media [5]; particularly, the nitrogen-doped carbon materials have been found to increase the ORR kinetics [6]. A brief comparison of the recently developed electrocatalysts for ORR is furnished in Table S1. There are several reports pertaining to high current density for acidic

Electronic supplementary material The online version of this article (https://doi.org/10.1007/s11581-020-03744-w) contains supplementary material, which is available to authorized users.

✉ S. Seetharaman
sraman25jd@gmail.com

Raghuram Chetty
raghuc@iitm.ac.in

[1] Department of Chemical Engineering, Indian Institute of Technology Madras, Chennai, India

fuel cells; however, there are fewer reports available on carbonaceous materials that integrate Fe and N into carbon with ORR performance comparable to that of Pt in alkaline media. The electrochemical performance and stability of such carbon materials in the alkaline medium are also not widely investigated.

Subsequent to the first report by Jasinski [7] that the cobalt phthalocyanine acts as an ORR catalyst in the alkaline medium, the focus of research turned towards other Co- and Fe-based N_4 macrocycles as ORR electrocatalysts. This was further substantiated by Bagotzky et al. [8] that the stability and activity of Co- and Fe-based N_4 macrocycles supported on carbon support could be improved by suitable heat treatments in an inert atmosphere. According to Gasteiger and Markovic [9], nitrogen-stabilized Fe or Co deposited on the high surface area carbon was found to exhibit enhanced oxygen reduction. According to various literature reports, pyrolysis of Fe and Co macrocycles adsorbed on a carbon surface through pyrolysis has demonstrated higher ORR activity [10–12].

The nature of nitrogen and transition metal functionalities on the carbon surface are responsible for the improved ORR activity, which is attributed to the formation of M-N_x (M = Fe, Co, etc.) moieties. These moieties are known to act as active sites for ORR and support in the adsorption/desorption of reaction intermediates [13–15]. Furthermore, the transitional metals like Fe act as a catalyst towards the graphitization of carbon. Besides, the Fe-N-C catalysts showed superior ORR activity by altering the nature of active sites which provides the 4e- pathway as described in the literature [16, 17]. In the light of the aforementioned, the present work is intended to investigate the ORR activity of the chemically reduced carbon xerogel and nitrogen-doped iron-coated graphene in alkaline media.

Indeed, the present research is focused on the development of NPMCs that are cost-effective and exhibit remarkable electrochemical activity, in order to replace the Pt electrocatalyst [18]. In particular, Fe-, Co-, and Ni-based oxides have been recently reported to exhibit high catalytic activities and are stable electrocatalysts [19]. Accordingly, various alternative electrocatalysts, such as metal-nitrogen-doped carbon materials, which are found to be the most promising candidates for ORR, were explored [20, 21]. Several reviews on such NPMCs have been reported, since the considerable activity of cobalt phthalocyanine towards ORR was described [22]. Pyrolysis of resorcinol-formaldehyde aqueous gels and their porous texture have been extensively studied and reported as an alternative catalyst support material in fuel cells [23–25]. This can be further optimized to obtain a series of carbon materials that possess a similar structure including pore size. Carbon xerogel (C_X) is a novel porous carbon that possesses a controllable mesoporous structure. Pekala et al. [26] reported a direct synthetic route to prepare ordered porous carbon materials through pyrolysis with suitable aromatic carbon precursors like resorcinol-formaldehyde resin. This method is widely recognized as a classical method to synthesize porous materials. Additional benefits of C_X pyrolysis include the abundance of the carbon source and improved electrical conductivity.

Accordingly, various kinds of carbon-supported and carbon-unsupported materials have been developed in the past decades, which include pyrolyzed transition metal with nitrogen-doped complexes, chalcogenides, transition metal/metal oxides/nitrides, and conducting polymer-based catalysts [27, 28]. Unfortunately, the ORR performance of these NPMCs was found to be lower than that of the existing Pt catalyst. Besides, it is challenging to control the physicochemical and morphological properties of these catalysts.

Graphene with its unique properties such as large surface area, increased conductivity, and electrochemical and thermal stability is particularly desirable as catalyst support material for fuel cell applications [29]. Recently, heteroatom-doped graphene received much attention owing to its improved activity and stability [30]. These graphene-based support materials are commonly prepared by reducing graphene oxide (rGO) via a chemical reduction method. It is noteworthy that the interaction of rGO materials plays a significant role in the conductivity of the overall catalyst.

In view of co-doping with two materials, one with higher electronegativity, while the other having lower electronegativity, viz., N having 3.04 and Fe having 1.83, compared with 2.55 for carbon, could create a favorable surface pattern by forming a unique charge transfer property with the coupling of a synergistic effect between these materials [31]. This effect appears to be a growing unanimity such that dual-doped catalysts with the addition of graphene make great potential in the design and tailoring of the physicochemical properties. Besides, these dual-doped catalysts exhibit superior performance for ORR than the individually doped graphene catalysts. In addition, the synergistic effect of dopants plays a vital role in ORR kinetics.

The present work reports the combination of high activity of reduced carbon xerogel-iron-nitrogen-doped graphene (rC_XFeNG) which can be prepared at low cost and is scalable, with high surface area and graphitic nature providing high current density. It is an effective way to control the electron donor properties and enhance the catalytic activities which suit ORR applications. Herein, we report that the hydrothermal carbonization of carbon xerogel with nitrogen-doped metal insertion followed by the addition of reduced graphene oxide leads to an enhanced ORR catalytic activity.

Experimental

Carbon xerogel synthesis

Carbon xerogel (C_X) was obtained by sol-gel polycondensation of resorcinol and formaldehyde (RF), in water, with

sodium carbonate as a catalyst using a preparation route reported elsewhere [26]. C_X is composed of an interconnected porous texture, the size of which depends on the ratios of resorcinol/catalyst and the pH. In a typical synthesis process, resorcinol (6.16 g) and formaldehyde (8.4 ml) were dissolved in 7 ml of deionized water. The polymerization of RF was initiated by the addition of sodium carbonate (0.02 mol/l) as a gelation agent. The mixture was stirred overnight and allowed to undergo gelation and aging initially in an oven at 60 °C for 8 h. Then, the resultant powder was placed in a quartz boat and placed inside a tubular furnace, which was subjected to pyrolysis at different temperatures such as 700, 900, and 1100 °C for 3 h in nitrogen atmosphere under a controlled heating program. The resultant powder was subjected to reduction using sodium borohydride to obtain reduced C_X.

Metal and nitrogen insertion

Incorporation of Fe and N into reduced C_X was carried out by using iron acetate and melamine as precursors, following the procedure proposed by Palanivelu and coworkers [32]. The total Fe loading was kept at 1.2 wt.% [24]. Briefly, 26 mg of iron acetate and about 200 mg of pyrolyzed C_X powder were dispersed in 30 ml of deionized water. The mixture was stirred overnight followed by quenching in liquid nitrogen. The resultant mixture was subjected to freeze-drying to yield a dry powder, which was heat treated at 800 °C under a nitrogen atmosphere. Melamine was added at this stage at a ratio of 3:2 (carbon-metal mixture:melamine). Then, the resultant mixture was packed in a vacuum-sealed quartz ampule and heat treated at 800 °C for 20 min. The black powder obtained after breaking the ampule is referred to as rC_XFeN.

Preparation of rC_XFeN-supported reduced graphene oxide

Reduced graphene oxide was synthesized via a modified Hummers' method according to our previous publications [33, 34]. The catalyst (rC_XFeN) was used for rGO addition. In the first step of the rC_XFeNG hybrid synthesis, the rC_XFeN aqueous solution was added into rGO/ethanol dispersion at room temperature. The reaction was stirred for 12 h at 60 °C followed by heating for 2 h at 80 °C. The resulting product was collected by centrifugation and finally dried at 60 °C. The catalyst samples were identified based on their pyrolysis temperature. The catalyst samples pyrolyzed at 700, 900, and 1100 °C were marked as rC_XFeNG-700, rC_XFeNG-900, and rC_XFeNG-1100, respectively.

Electrochemical measurements

The electrochemical behavior and the ORR activity of the as-prepared electrocatalysts were assessed through cyclic voltammetry and linear sweep voltammetry using a rotating disk electrode (RDE). In brief, the experiment was performed in a three-electrode setup with a saturated Ag/AgCl electrode as a reference electrode. The potentials quoted in this work are converted to the reversible hydrogen electrode (RHE) scale unless otherwise specified. The catalyst-coated RDE tip and platinum coil were used as the working and counter electrodes, respectively. The working electrode was prepared by drop-casting the catalyst ink onto the RDE. In brief, about 4 mg of sample was ultrasonically dispersed in 0.7 ml of water, 0.3 ml of ethanol, and 10 μl of Nafion 5 wt.% ionomer [35]. The resultant catalyst suspension was coated on a 3-mm-diameter disk such that the catalyst loading remained 0.5 mg cm^{-2} in all cases. Measurements on an RDE were carried out on an electrode rotator (Pine Instrument) and the CHI 760D potentiostat. The LSV (linear sweep voltammetry) measurements were recorded at various rotation speeds from 400 to 2000 revolutions per minute (rpm) at a scan rate of 5 mV s^{-1} in 0.1 M KOH. Prior to testing the ORR activity, LSV was run in a nitrogen-purged electrolyte and taken as a baseline, followed by running the same in oxygen-saturated 0.1 M KOH. In addition, the electrochemical stability of the designated electrocatalysts was assessed by potential cycling of the catalyst-coated electrodes between − 0.1 and 0.2 V vs. Ag/AgCl in 0.1 M KOH. For effective comparison, the commercial 10 wt.% Pt/C catalyst (Johnson Matthey) was also studied with the same catalyst loading under identical conditions.

Physical characterizations

Scanning electron microscopy (SEM) micrographs were acquired using a Hitachi S-4800 instrument. Powder X-ray diffraction (XRD) was recorded using a PANalytical X'Pert Pro X-ray diffractometer with Cu Kα radiation as the X-ray source. FT-Raman spectra were carried on a Bruker RFS 27 instrument with 514.3-nm Ar laser with a power of 10 mW. X-ray photoelectron spectroscopy (XPS) measurements were carried with a Thermo Fisher Scientific ESCALAB 250 XPS system, using a monochromated Al Kα source with a power of 15 keV used for determining the oxidation states and chemical bonding of constituent elements. The thermogravimetric analyses (TGA) of all the catalysts were recorded by TA Instruments SDT Q600 under air atmosphere, heating up to 1200 °C at a rate of 10 °C per minute.

Results and discussion

XRD analysis

XRD was used to study the crystallinity and spacing between the graphitic planes of the heat-treated samples. Figure 1 shows XRD patterns for the as-prepared electrocatalysts with peaks at around 26° and 43° corresponding to the {002} and {101} planes of the graphitic carbon. In addition, similar but broader peaks are also observed for rC_XFeNG-700 and rC_XFeNG-900, which may be ascribed to the lower graphitization of carbon xerogel. However, in the case of rC_XFeNG-1100, the peaks at 26° appear to be sharper which clearly shows the crystalline nature of graphitic carbon having a lesser number of surface defects. This is because high-temperature pyrolysis could significantly improve the degree of graphitization and enhance the maximum utilization of available active sites [36]. Moreover, there were no detectable Fe peaks in the spectra, implying that the Fe particles might be incorporated into the graphitic carbon framework.

FT-Raman

Figure 2 shows Raman spectra for rC_XFeNG-700, rC_XFeNG-900, and rC_XFeNG-1100 electrocatalysts. The Raman peaks at 1356 and 1580 cm^{-1} are attributed to the disordered and graphitic carbon structures, respectively. The ratios of the intensity of the disordered and graphitic carbon (I_D/I_G) for rC_XFeNG-700, rC_XFeNG-900, and rC_XFeNG-1100 electrocatalysts are found to be 1.19, 1.11, and 1.08, respectively. The decrease in the I_D/I_G ratio with an increase in pyrolysis temperature of the C_X is due to the more ordered

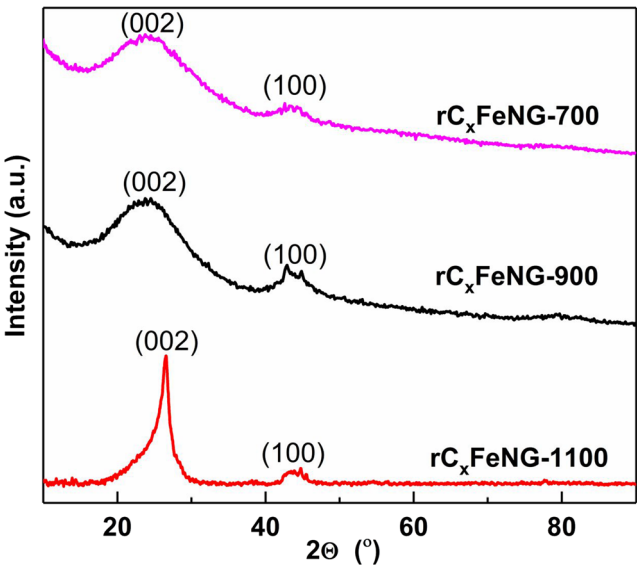

Fig. 1 XRD pattern of rC_XFeNG catalysts

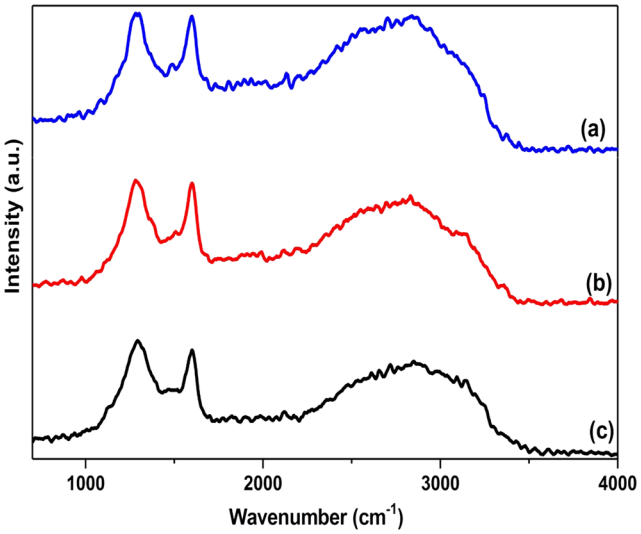

Fig. 2 Raman spectrum for rC_XFeNG catalysts: (a) rC_XFeNG-700, (b) rC_XFeNG-900, and (c) rC_XFeNG-1100

graphitic structure with a lesser number of defects. This indicates the relation between the surface defects and degree of graphitization with temperature. Moreover, the results from Raman spectra are akin to the XRD results. Since the defect concentration is lower in rC_XFeNG-1100, the conductivity is expected to be better than the other samples. This variation in crystallinity matches well with XRD results and reports for the comparatively high electrical conductivity of rC_XFeNG-1100.

HR-SEM

To study the effect of pyrolysis temperature on the ORR performance, the morphology of the catalysts was studied using HR-SEM as shown in Fig. 3. The HR-SEM images reveal the effect of temperature on the morphology of the catalysts related to the nature of pores formed on the surface. Catalysts pyrolyzed at 1100 °C exhibit alveolar, interconnected, and porous structures. Efficient electron transport in rC_XFeNG-1100 catalysts pyrolyzed at 1100 °C is expected, owing particularly to the interconnected chain network of prominent domains.

Comparing the HR-SEM micrographs of the various electrocatalysts, it is noticeable that there is an increase in smaller particle dimensions for the rC_XFeNG-1100 electrocatalyst in addition to the observed porous structure. This is attributed to the availability of more anchoring sites with high-temperature pyrolysis and more number of particles embedded in graphene providing a higher surface area catalyst framework. This is advantageous for the permeability of the reactant molecules and reaches the ionomer electrolyte interphase. Figure S1 shows the EDX data, which confirms the presence of C, N, and Fe in the catalysts with no other impurities detected. It can be observed that the Fe nanoparticles are dispersed consistently over the supporting medium.

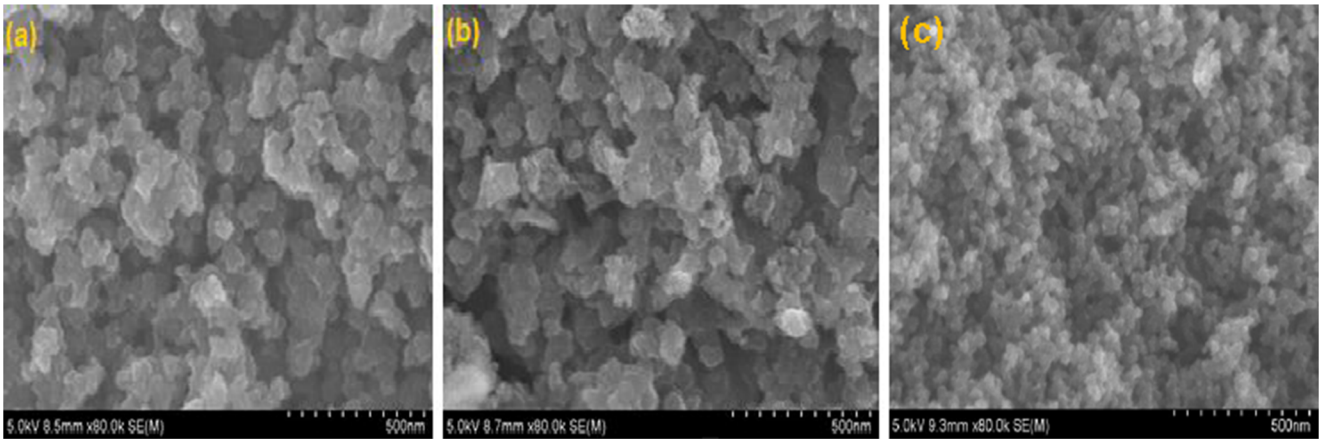

Fig. 3 HR-SEM micrographs of rC_XFeNG catalysts: (**a**) rC_XFeNG-700, (**b**) rC_XFeNG-900, and (**c**) rC_XFeNG-1100

TEM and BET

Figure 4 shows the TEM images for the rC_X, rC_XFeN, and rC_XFeNG catalysts. It is observed that co-doping of Fe and N to the rGO caused unzipping of the graphene sheets resulting in a wrinkled /exfoliated structure as observed in Fig. 4(c). Figure S2 shows the high-magnification TEM images of rC_XFeNG catalysts, which are homogeneously distributed.

The BET surface area of rC_XFeNG has been recorded as 404.5 $m^2\ g^{-1}$ as compared with that of rC_X (296.4 $m^2\ g^{-1}$) as tabulated in Table 1, indicating the benefits of nitrogen doping and graphene addition. N doping provides high electron mobility and enhances the dispersion of metal deposition [11], whereas addition of graphene nanosheets as a supporting medium offers a high specific surface area and large pore volume, resulting in a further increase in the dispersion of FeN on the graphene structure [37], due to which an increase in surface area was observed. The BET surface area results are akin to the confirmation drawn from the HR-SEM and TEM analyses.

Besides, micropores present in the surface of the rC_X increased drastically from 337 to 450 $m^2\ g^{-1}$ for rC_XFeNG as furnished in Table 1. These micropores are considered crucial for the ORR activity and are directly correlated with ORR activity in the literature [30, 34]. Thus, embedding the designated catalysts onto a graphene sheet to form a composite framework is beneficial due to the ensuing properties such as increased surface area and pore size as well as pore volume.

XPS

XPS spectra confirm the incorporation of nitrogen on the carbon xerogel rC_XFeNG-1100 sample as shown in Fig. 5(a, b). These C1s spectra were deconvoluted into four components. The contribution at 285.5–285.8 eV and 284.6–284.9 eV can be assigned to the presence of the C–C and C–O bonds. The peaks at 286.1–286.5 eV and 283.8–284.2 eV confirm the presence of the C–N and C=C bonds. Figure 5(b) shows the N1s spectra for rC_XFeNG-1100, deconvoluted into three components at 399.05, 400.02, and 401.38 eV, which are attributed to the pyridinic, pyrrolic, and graphitic nitrogen, respectively. XPS data suggested the presence of 1.6 wt.% nitrogen in the overall sample. The neutral amine peaks could have disappeared due to the higher pyrolysis temperature of 1100 °C [20]. The total Fe content in the overall catalyst

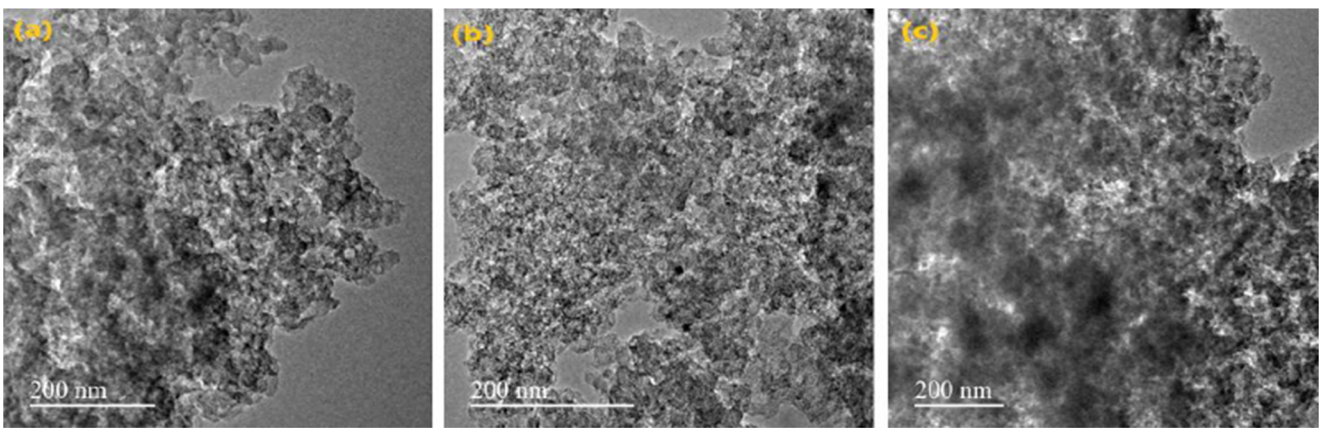

Fig. 4 TEM images of the (**a**) rC_X, (**b**) rC_XFeN, and (**c**) rC_XFeNG catalysts

Table 1 BET-related information about the rC_X, rC_XFeN, and rC_XFeNG catalysts

Samples	BET surface area ($m^2\ g^{-1}$)	Micropore surface area ($m^2\ g^{-1}$)	*t*-plot micropore volume ($cm^3\ g^{-1}$)	Avg. pore width (Å)
rC_X	296.4	337.2	0.596	64.5
rC_XFeN	352.4	433.1	0.646	73.4
rC_XFeNG	404.5	450.9	0.861	85.1

was maintained at 1.2 wt.%, over which the rGO was added, due to which the presence of Fe could not have been detected in the XPS spectra. Charreteur and co-workers [38] also made similar observations on the porphyrin-based carbon black catalyst where peaks corresponding to Fe were not detected in the XPS spectra, which was attributed to the Fe crystals covered by graphitic carbon impeding Fe detection in the XPS technique. The incorporation of nitrogen in terms of graphitic, pyrrolic, and pyridinic "N," enhances the bonding ability of the adjacent atoms which could provide a well-conductive pathway for the transfer of electrons. It is well known that the presence of graphitic, pyrrolic, and pyridinic nitrogen improves the ORR activity since the presence of nitrogen functionalities is directly propositional to ORR kinetics.

The equal content of pyridinic, pyrrolic, and graphitic nitrogen, which was proposed to create a positive charge density on the adjacent edge plane, has been certainly related to the ORR activity [36]. On the other hand, the C1s spectrum in Fig. 5(a) could also be deconvoluted into the asymmetric peaks, indicating the formation of sp^2 hybridized carbon atoms.

TGA profiles for rC_XFeNG-700, rC_XFeNG-900, and rC_XFeNG-1100 are shown in Fig. 6; rC_XFeNG-700 and rC_XFeNG-900 exhibited the first decomposition temperature at around 550 °C, whereas for rC_XFeNG-1100, the first decomposition was observed at a higher temperature of around 800 °C. The thermal decomposition behavior of all the materials showed a two-step weight loss. The first step was due to the moisture contained in each sample, whereas the second step corresponds to the main thermal decomposition of the material. These data indicate the influence of temperature on the decomposition process, where decreasing the pyrolysis temperature increases the decomposition rate. It can be observed that rC_XFeNG-1100 shows higher thermal stability than the rC_XFeNG-700 and 900 frameworks.

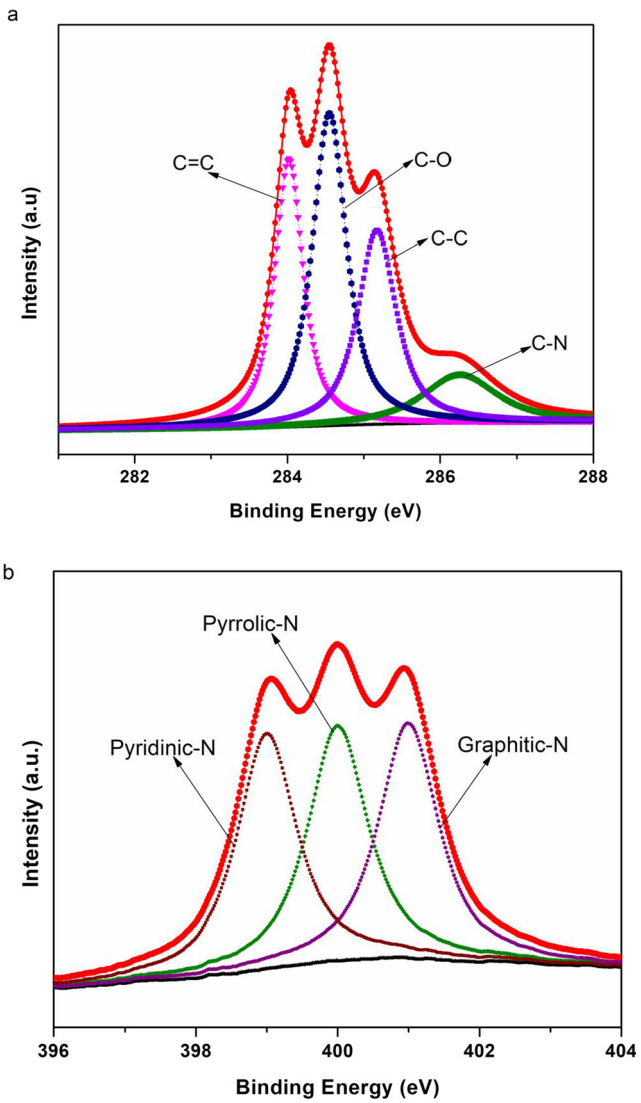

Fig. 5 **a** Deconvoluted C1s XPS spectra for rC_XFeNG-1100 catalysts. **b** Deconvoluted N1s XPS spectra for rC_XFeNG-1100 catalysts

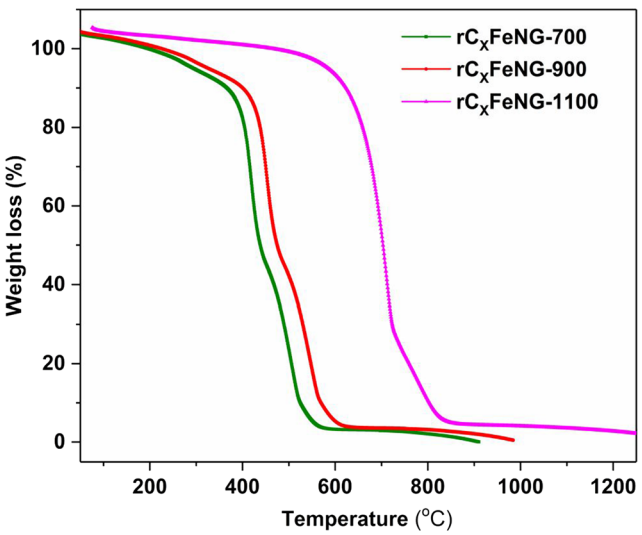

Fig. 6 TGA plot for rC_XFeNG catalysts

Electrochemical characterization

The electrocatalytic activity of all the samples was tested by the RDE setup with linear sweep voltammetry (LSV) and cyclic voltammetry (CV) in O_2- and N_2-saturated 0.1 M KOH solution. To ensure fairness and for a better understanding of the catalytic performances of the synthesized rC_XFeNG catalysts, all the catalyst inks were prepared by the same procedure with identical loadings. Before recording the ORR current, LSV was run with the N_2-saturated electrolyte to measure the background current which was then used to normalize the kinetic current. Figure 7 shows the LSV-ORR curves for the rC_XFeNG-700, rC_XFeNG-900, rC_XFeNG-1100, and commercial Pt/C electrocatalysts. Among the various electrocatalysts, the lowest performance was observed for rC_XFeNG without heat treatment, indicating the effect of pyrolysis temperature on the overall performance.

After pyrolysis at 700 °C, the catalyst showed little improvement in the activity, entailing that the effect of temperature has an impact. As the pyrolysis temperature increased, the surface-bound functionalities change drastically; this could modify the shapes and create several catalytic active sites [39]. The rC_XFeNG-1100 had the highest peak current density of 5.55 mA cm^{-2}, which was about fourfold as compared with that of rC_XFeNG-700. In contrast, the Pt/C showed a peak current density of 3.83 mA cm^{-2}, although the onset potential for Pt/C was superior to the designated catalysts. Thus, the rC_XFeNG-1100 electrocatalyst with xerogel heat treated at an optimum temperature of 1100 °C shows higher performance among the electrocatalysts studied as evidenced by the LSV data. It is noteworthy that albeit the higher capacitance current observed for rC_XFeNG-1100, the capacitance current is negligible compared with the ORR current. Moreover, the LSVs were run on variable rotation speeds to eliminate the capacitance contribution, and the kinetic current observed in each rotation rate for rC_XFeNG-1100 was superior to its counterparts and comparable to that of Pt/C.

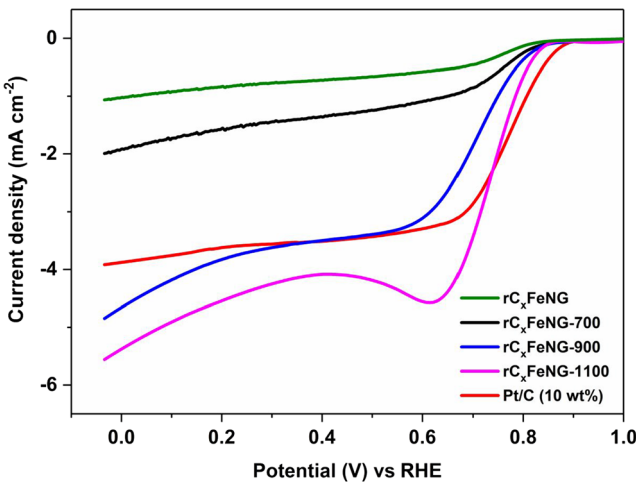

Fig. 7 Comparative LSV plots for the Pt/C and rC_XFeNG electrocatalysts in O_2-saturated 0.1 M KOH solution at a scan rate of 5 mV/s and rotation speed of 1600 rpm

The performance of the rC_XFeNG-1100 catalyst is the highest for ORR among the electrocatalysts prepared, which may be ascribed to the enhanced utilization of active sites and also the effect of π-π stacking [28]. As a result, the onset potential increases with increasing pyrolysis temperature. The size of the π-π stacking is dependent upon the pyrolysis temperature, and as proposed by Chen et al. [30], the structure of active sites is responsible for the high activity in Fe-N-C ORR catalysts. The above experimental results strongly suggest that the synergistic mechanism in the case of rC_XFeNG and also the effect of high-temperature pyrolysis could significantly increase the surface charge density of Fe-N_x configuration and thus enhance its ORR performance.

To gain more information on the ORR kinetics of the rC_XFeNG-1100 catalyst, LSV was carried out at various rotation rates ranging from 400 to 2000 rpm as shown in Fig. S3. It is observed that the current density increases with an increase in rpm, due to an increase in electron transfer kinetics. Besides, the mass transfer kinetics could improve with an increase in rotation speed. The high current density of −5.55 mA cm^{-2} measured at 0.72 V vs. RHE was obtained under the rotation rate of 1600 rpm, whereas it shows −6.3 mA cm^{-2} at 2000 rpm. The diffusion current increases with the increase in the rotation rate. Figure S4 shows the ORR curves of all the ingredients of the rC_XFeNG sample without pyrolysis, which suggests that reduced carbon xerogel performs better than the pure carbon xerogel due to the availability of more anchoring sites in the reduced form. Moreover, the addition of iron, nitrogen, and reduced graphene oxide co-doping can greatly enhance the coordination bond of Fe-N-C. The addition of graphene can increase the surface area, which contributes to the increase in active sites with effective charge transfer capability. The addition of surface nitrogen could increase the active site density and enhance the ORR performance through improved reaction kinetics. Reduced GO in the catalyst framework may provide the benefit of acting as a charge carrier resulting in higher conductivity and offers stability to the framework structure, especially protecting the active sites of Fe from leaching.

Figure 8 shows the CV curves of all the electrocatalysts, which revealed that rC_XFeNG-1100 maintains the highest electrochemical activity due to the diminution in the resistance by removing the oxygenated surface groups and showed improvement in mass transfer behavior. In contrast, the low activity of rC_XFeNG may be due to the weak bonding of the intermediate species. An increase in the pyrolysis temperature led to a clear enhancement of the electron transfer kinetics of ORR. Furthermore, the *K-L* plot shown in Fig. 9 at different electrode potentials is in good agreement with the CV and LSV curves. From the *K-L* plots, the ORR processes on

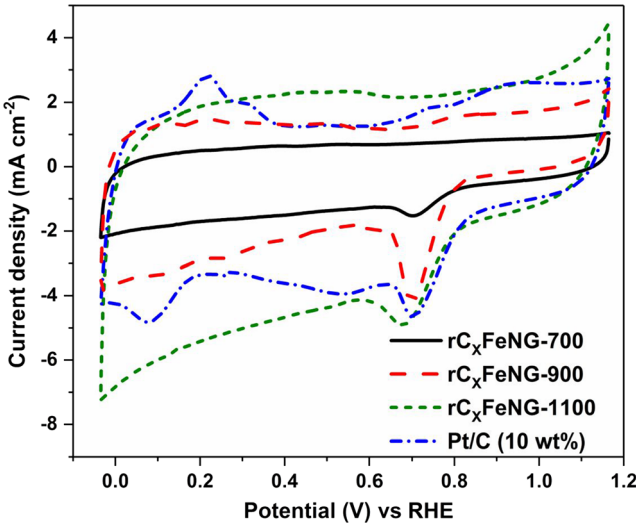

Fig. 8 Cyclic voltammograms for the Pt/C and rC_XFeNG electrocatalysts in O_2-saturated 0.1 M KOH at a scan rate of 5 mV/s

rC_XFeNG-1100 catalysts are observed to follow a four-electron reduction pathway ($n = 3.94$) in the high potential range through dual-site mechanisms [15].

From the electrochemical characterizations, it can be confirmed that the catalytic performance of rC_XFeNG-1100 is close to that of commercial Pt/C (10 wt.%). Further, the onset potential of rC_XFeNG-1100 is slightly shifted to positive by 0.11 V than that of Pt/C. The ORR onset of our catalyst can be correlated to the $Fe^{2+/3+}$ redox peaks [40]. The behavior of rC_XFeNG-1100 shows that the increase in the peak current density may result in an enhancement in the number of additional active sites available for adsorption and desorption of reactant intermediates during the ORR.

EIS for various synthesized electrocatalysts was carried out to measure the resistance due to the variation in the catalyst as well as support structure, and the data are presented in Fig. S5.

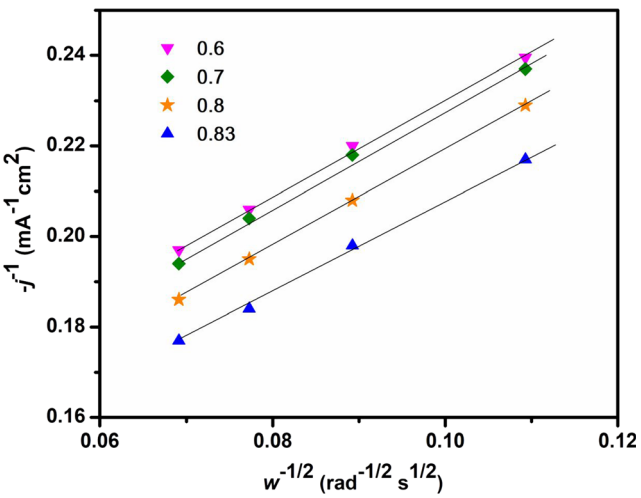

Fig. 9 *K-L* plots for rC_XFeNG-1100 electrocatalyst at various potentials vs. RHE

It is clear from the Nyquist plot that the resistance of pure rC_XFeNG is about 9 times higher than that of rC_XFeNG-1100 samples. It is surprising to notice such remarkable differences in the reduced samples. The inset in Fig. S5 depicts the impedance behavior of all the as-synthesized catalysts at high frequencies. The rC_XFeNG-1100 shows lower impedance compared with those pyrolyzed samples at 700 and 900 °C (i.e., rC_XFeNG-700 and rC_XFeNG-900), which is in good agreement with the LSV and CV curves. This could correlate with an increase in the conductivity of the reduced samples having a large number of active sites accessible to the reaction medium [41]. Hence, it could enhance the ORR performance.

Durability

A durability study was carried out by potential cycling of the catalyst-coated electrode between − 0.1 and 0.2 V vs. Ag/AgCl in 0.1 M KOH, which were then converted into the RHE scale. Before the durability study, rC_XFeNG-1100 catalysts exhibited an exceptional ORR activity as shown in Fig. 10. It shows an onset potential of 0.84 V vs. RHE and half-wave potential ($E1/2$) of ~0.72 V. Interestingly, even after 4000 continuous cycles, only a small decrease in current density was observed and the $E1/2$ positively shifted by ~0.72 V.

This strongly suggests that the individual ingredients were not leached away into the electrolyte throughout the cycling. These results also show the higher stability of the catalyst in alkaline solution. Besides, the graphene nanosheets, known for their electrochemical stability, act as a stable backbone for the reduced carbon xerogel matrix which could considerably mitigate the degradation and leaching of Fe and N during the long-term operation.

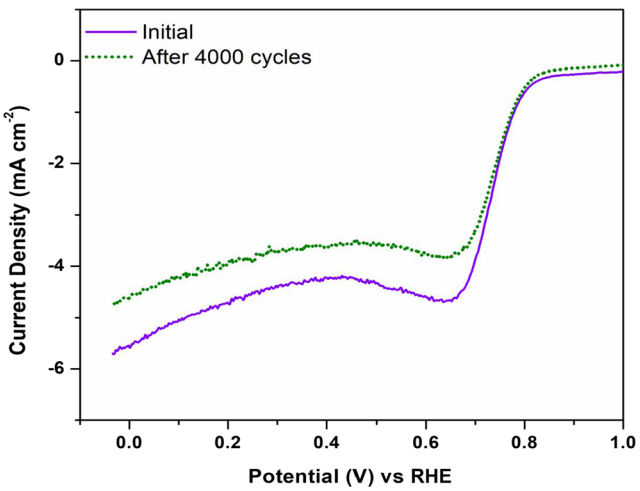

Fig. 10 Durability performance of rC_XFeNG-1100 electrocatalyst: before and after 4000 potential cycles in O_2-saturated 0.1 M KOH

The enhanced ORR catalytic activity of the rC_XFeNG-1100 catalyst is assigned to the synergistic combination of the reduced carbon xerogel, nitrogen, and iron co-doped with reduced graphene oxide at the higher pyrolysis temperature, which can pave the way to the efficient design and fabrication of cost-effective non-precious ORR electrocatalysts for alkaline polymer electrolyte fuel cells.

Conclusions

In the present work, an attempt was made to design and synthesize a high-performance NPMC for ORR in the alkaline media. It is observed that through an effective heat treatment, the chemically reduced carbon xerogel with a mixture of nitrogen and iron co-doped with reduced graphene oxide prepared via a facile synthesis method showed enhanced catalytic activity towards ORR. The consolidation of reduced carbon xerogel with nitrogen-doped iron-coated graphene urges the formation of a conducting network, which facilitates the charge transfer process during the electrochemical reactions. Moreover, with an increase in pyrolysis temperature, a higher degree of graphitization was achieved, which in turn improved the electronic conductivity of the designated catalyst. The rC_XFeNG-1100 framework formed on carbon xerogel pyrolyzed at 1100 °C clearly showed the four-electron transfer mechanism for ORR similar to that of Pt/C. It is observed that the rC_XFeNG-1100 showed an onset potential of 0.84 V vs. RHE, a higher limiting current density of − 5.55 mA cm^{-2}, and a half-wave potential ($E1/2$) of ~0.72 V vs. RHE among the other catalysts. Besides, the rC_XFeNG-1100 framework electrocatalyst exhibited improved durability of up to 4000 potential cycles with minimum loss in performance. The substantial increment in the ORR activity and durability of the rC_XFeNG-1100 catalyst is explained based on the synergistic effect between the strong coordination bonds of Fe-N-C and the active sites that drastically increase with the pyrolysis temperature. Moreover, graphene as support around the reduced carbon xerogel matrix prominently mitigates the leaching of Fe and N resulting in enhanced long-term stability. The significant improvement in ORR activity and durability of rC_XFeNG-1100 is attributed to the synergistic effect between the strong coordination bonds of Fe-N-C and the active sites on the framework that drastically increase with increase in pyrolysis temperature. This rational design of high-performance catalysts opens the door for the possibility of exposing cost-effective ORR catalysts for fuel cell applications.

Acknowledgments We acknowledge DST-FIST for providing the instrumentation facility to the Department of Chemical Engineering, IIT Madras.

Funding information The authors would like to thank the Indian Institute of Technology (IIT) Madras for the financial support under the Institute Postdoctoral Fellowship Scheme to S. Seetharaman. The authors are thankful to the Science and Engineering Research Board (SERB), Department of Science and Technology (DST), Government of India, for providing the financial support to S. Vinod Selvaganesh (PDF/2016/002945) under the National Postdoctoral Fellowship Scheme.

References

1. Cifrain M, Kordesch KV (2004) Advances, aging mechanism and lifetime in AFCs with circulating electrolytes. J Power Sources 127: 234–242
2. Varcoe JR, Slade RCT (2005) Prospects for alkaline anion-exchange membranes in low temperature fuel cells. Fuel Cells 5: 187–200
3. JOM, Bockris SS (1969) Fuel cells: their electrochemistry. 289–291
4. Wu CY, Wu PW, Lin P, Li YY, Lin YM (2007) Silver-carbon nanocapsule electrocatalyst for oxygen reduction reaction. J Electrochem Soc 154:B1059–B1062
5. Guo D, Shibuya R, Akiba C, Saji S, Kondo T, Nakamura J (2016) Active sites of nitrogen-doped carbon materials for oxygen reduction reaction clarified using model catalysts. Science 351:361–365
6. Nallathambi V, Leonard N, Kothandaraman R, Barton SC (2011) Nitrogen precursor effects in iron-nitrogen-carbon oxygen reduction catalysts. Electrochem Solid-State Lett 14:B55–B58
7. Jasinski R (1964) A new fuel cell cathode catalyst. Nature 201: 1212–1213
8. Bagotzky VS, Tarasevich MR, Radyushkina KA, Levina OE, Andrusyova SI (1977) Electrocatalysis of the oxygen reduction process on metal chelates in acid electrolyte. J Power Sources 2: 233–240
9. Gasteiger HA, Markovic NM (2009) Just a dream-or future reality. Science 324:48–49
10. Biloul A, Gouerec P, Savy M, Scarbeck G, Besse S, Riga J (1996) Oxygen electrocatalysis under fuel cell conditions: behaviour of cobalt porphyrins and tetraazaannulene analogues. J Appl Electrochem 26:1139–1146
11. Peera SG, Kwon HJ, Lee TG, Hussain AM (2020) Heteroatom- and metalloid-doped carbon catalysts for oxygen reduction reaction: a mini-review. Ionics 26:1563–1589
12. Sawaguchi T, Itabashi T, Matsue T, Uchida I (1990) Electrochemical reduction of oxygen by metalloporphyrin ion-complexes with heat treatment. J Electroanal Chem 279:219–230
13. Seul L, Hee KD, Beom HS, Tak HE, Cheol KM, Yeon LJ, Woo LY (2016) Synthesis of hollow carbon nanostructures as a non-precious catalyst for oxygen reduction reaction. Electrochim Acta 191:805–812
14. Duan J, Zheng Y, Chen S, Tang Y, Jaroniec M, Qiao S (2013) Mesoporous hybrid material composed of Mn_3O_4 nanoparticles on nitrogen-doped graphene for highly efficient oxygen reduction reaction. Chem Commun 49:7705–7707
15. Ali RM, Hassan OH, Ali AM, Taib MFM, Yahya MZA (2020) Electrochemical properties of pyrolysed graphene/activated carbon composite doped with FeTMPP-Cl as electrode materials. Ionics. 26:2825–2834. https://doi.org/10.1007/s11581-020-03533-5
16. Qiao X, You C, Shu T, Fu Z, Zheng R, Zeng X, Li X, Liao S (2014) A one-pot method to synthesize high performance multielement co-

doped reduced graphene oxide catalysts for oxygen reduction. Electrochem Commun 47:49–53
17. Zhao Q, Ma Q, Pan F, Guo J, Zhang J (2016) Facile synthesis of N-doped carbon nanosheet-encased cobalt nanoparticles as efficient oxygen reduction catalysts in alkaline and acidic media. Ionics 22: 2203–2212
18. Bashyam R, Zelenay P (2006) A class of non-precious metal composite catalysts for fuel cells. Nature 443:63–66
19. Zhao Y, Fan R, Chen Z, Zhao Q, Li J, Yang L, Xue J (2018) Engineering beneficial structures and morphologies of M-N-C oxygen-reduction catalysts derived from different metal-containing precursors. Ionics 24:1733–1744
20. Anjaiah S, Sudip M, Thirupathi T, Ramkumar V, Kothandaraman R (2016) Carbon-supported Co(III) dimer for oxygen reduction reaction in alkaline medium. Ionics 22:2183–2194
21. Shaofang F, Chengzhou Z, Yazhou Z, Guohai Y, Won J, John L, Dan D, Satish KN, Yuehe L (2015) Metal-organic framework derived hierarchically porous nitrogen-doped carbon nanostructures as novel electrocatalyst for oxygen reduction reaction. Electrochim Acta 178:287–293
22. Jasinski R (1965) Cobalt phthalocyanine as a fuel cell cathode. J Electrochem Soc 112:526–528
23. Nagaiah TC, Kundu S, Bron M, Muhler M, Schuhmann W (2010) Nitrogen-doped carbon nanotubes as a cathode catalyst for the oxygen reduction reaction in alkaline medium. Electrochem Commun 12:338–341
24. Selvarani G, Nathaniel L, Barton SC (2014) Impact of transition metal on nitrogen retention and activity of iron-nitrogen-carbon oxygen reduction catalysts. Phys Chem Chem Phys 16:4576–4585
25. Xu S, Zhang Z, Wu T, Xue Y (2018) Nanoporous carbon microspheres as anode material for enhanced capacity of lithium ion batteries. Ionics 24:99–109
26. Pekala RW, Farmer JC, Alviso CT, Tran TD, Mayer ST, Miller JM, Dunn BJ (1998) Carbon aerogels for electrochemical applications. Non-Cryst Solids 225:74–80
27. Gong K, Du F, Xia Z, Durstock M, Dai L (2009) Nitrogen-doped carbon nanotube arrays with high electrocatalytic activity for oxygen reduction. Science 323:760–764
28. Choi CH, Park SH, Woo SI (2012) Binary and ternary doping of nitrogen, boron, and phosphorus into carbon for enhancing electrochemical oxygen reduction activity. ACS Nano 6:7084–7091
29. Thapa BS, Seetharaman S, Chetty R, Chandra TS (2019) Xerogel-based catalyst for improved cathode performance in microbial fuel cells. Enzym Microb Technol 124:1–8
30. Chen Y, Sun L, Lu Z, Liu Z, Jiang Y, Zhuo K (2019) Preparation of nitrogen and sulfur co-doped graphene aerogel with hierarchical porous structure using ionic liquid precursor for high-performance supercapacitor. Ionics 25:2781–2789
31. Holade Y, Sahin NE, Servat K, Napporn TW, Kokoh KB (2015) Recent advances in carbon supported metal nanoparticles preparation for oxygen reduction reaction in low temperature fuel cells. Catalysts 5:310–348
32. Palanivelu KM, Prabhakaran V, Ramani VK, Ramanujamam K (2015) Controlling the nitrogen content of metal-nitrogen-carbon based non-precious-metal electrocatalysts via selenium addition. J Electrochem Soc 162:F475–F482
33. Seetharaman S, Raghu S, Velan M, Ramya K, Ansari K (2015) Comparison of the performance of reduced graphene oxide and multiwalled carbon nanotubes based sulfonated polysulfone membranes for electrolysis application. Polym Compos 36:475–481
34. Sarkar IJR, Peera SG, Chetty R (2018) Manganese oxide nanoparticles supported nitrogen-doped graphene: a durable alkaline oxygen reduction electrocatalyst. J Appl Electrochem 48:849–865
35. Yao F, Pham DT, Lee YH (2015) Carbon-based materials for lithium-ion batteries, electrochemical capacitors, and their hybrid devices. Chem Sus Chem 8:2284–2311
36. Xiang Z, Xue Y, Cao D, Huang L, Chen JF, Dai L (2014) Highly efficient electrocatalysts for oxygen reduction based on 2d covalent organic polymers complexed with non-precious metals. Angew Chem Int Ed 53:2433–2437
37. Vinod Selvaganesh S, Dhanasekaran P, Chetty R, Bhat SD (2019) Microwave assisted poly(3,4-ethylenedioxythiophene)-reduced graphene oxide nanocomposite supported Pt as durable electrocatalyst for polymer electrolyte fuel cells. New J Chem 42: 10724–10732
38. Charreteur F, Jaouen F, Dodelet J-P (2009) Iron porphyrin-based cathode catalysts for PEM fuel cells: influence of pyrolysis gas on activity and stability. Electrochim Acta 54:6622–6630
39. Zhang LS, Liang XQ, Song WG, Wu ZY (2010) Identification of the nitrogen species on N-doped graphene layers and Pt/NG composite catalyst for direct methanol fuel cell. Phys Chem Chem Phys 12:12055–12059
40. Niu W, Li L, Liu X, Wang N, Liu J, Zhou W, Tang Z, Chen S (2015) Mesoporous N-doped carbons prepared with thermally removable nanoparticle templates: an efficient electrocatalyst for oxygen reduction reaction. J Am Chem Soc 137:5555–5562
41. Yin H, Zhang C, Liu F, Hou Y (2014) Hybrid of iron nitride and nitrogen-doped graphene aerogel as synergistic catalyst for oxygen reduction reaction. Adv Funct Mater 24:2930–2937